Supplementary Information: One-dimensional quantum channel in bent honeycomb nanoribbons

Tong Wang,[1] Xi Jiang,[1] Jing Wang,[1] Zhao Liu,[1,2,*] Juntao Song,[1,†] and Ying Liu[1,3]

[1] *Department of Physics and Hebei Advanced Thin Film Laboratory, Hebei Normal University, Shijiazhuang 050024, Hebei, China*
[2] *Beijing Computational Science Research Center, Beijing 100193, China*
[3] *National Key Laboratory for Materials Simulation and Design, Beijing 100083, China*

I. WAVE FUNCTIONS FOR OTHER BENT ZIGZAG NANORIBBONS AT $\kappa = 0.7\pi$

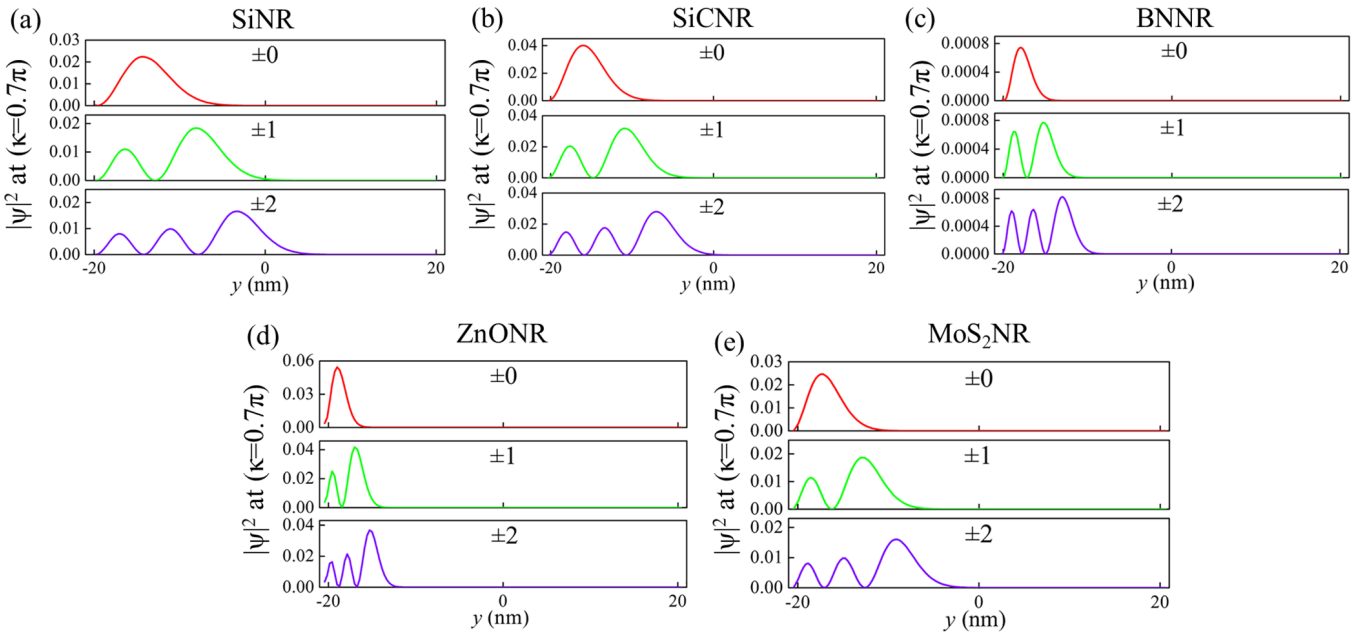

FIG. S1. Spatial distributions of wave functions at $\kappa = 0.7\pi$ along width direction y for the first three LLs ($n = \pm 0, \pm 1, \pm 2$) of bent zigzag (a) SiNR, (b) SiCNR, (c) BNNR, (d) ZnONR, and (e) MoS_2NR. The wave functions in red, green, and purple colors corresponding to the bands highlighted with the same colors as shown in the manuscript.

In the manuscript, we only show the wave functions of bent zigzag GNR at $\kappa = 0.7\pi$. Here we also show the spatial distributions of wave functions corresponding to the first three LLs near the Fermi level for bent zigzag SiNR, SiCNR, BNNR, ZnONR, and MoS_2NR at $\kappa = 0.7\pi$, as shown in Fig. S1. Same as the Landau electronic states at $\kappa = 0$, the nodes of the wave functions at $\kappa = 0.7\pi$ also conform to the numbering rule of the LLs. Moreover, the electronic states at $\kappa = 0.7\pi$ are localized on the other side of the NRs, close to the innermost edge of the bent NRs.

II. ELECTRONIC BAND STRUCTURES AND WAVE FUNCTIONS OF ARMCHAIR NANORIBBONS AT DIFFERENT BENDING ANGLES

In the manuscript, we show the energy bands and wave functions of 6 kinds of bent zigzag NRs. Here, we similarly show the electronic band structures and wave functions at $\kappa = \pi$ of bent armchair GNR, SiNR, SiCNR, BNNR, ZnONR, and MoS_2NR, as shown in Figs. S2-S7.

As shown in Fig. S2(a), the strain-free armchair GNR [1] is a 2D material with zero band gap. Under bending, the CBs shift down and the VBs shift up. Moreover, the wave functions of bent GNR are well localized at the edge of the NR, see Fig. S2(b). Similar to zigzag GNR, the number of nodes of the localized electronic states also meets the rule of LL index.

As shown in Fig. S3(a), the strain-free armchair SiNR [2] is a 2D material with zero band gap like armchair GNR. Under bending, the CBs shift down and the VBs shift up. Moreover, the wave functions of bent SiNR are well localized at the edge of the NR, see Fig. S3(b). Similar to zigzag NRs, the number of nodes of the localized electronic states also meets the rule of LL index.

As shown in Fig. S4(a), the strain-free armchair SiCNR [3] has a direct band gap about 1.54 eV. Under bending, the CBs shift down and VBs shift up, leading to a reduced band gap about 1.23 eV. Moreover, the wave functions of bent SiCNR are well localized at the edge of the NR, see Fig. S4(b). Similar to zigzag NRs, the number of nodes of the localized electronic states also meets the rule of LL index.

As shown in Fig. S5(a), the strain-free armchair BNNR [4] has a direct band gap about 3.96 eV. Under bending, both the CBs and the VBs shift down, leading to a reduced band gap about 3.77 eV. Moreover, the wave functions of bent BNNR are well localized at the edge of the NR, see Fig. S5(b). Similar to zigazg NRs, the number of nodes of the localized electronic states also meets the rule of LL index.

As shown in Fig. S6(a), the strain-free armchair ZnONR [5] has a direct band gap about 4.50 eV. Under bending, both the CBs and VBs shift down, leading to a reduced band gap about 4.16 eV. Moreover, the wave functions of bent ZnONR are well localized at the edge of the NR, see Fig. S6(b). Similar to zigzag NRs, the number of nodes of the localized electronic states also meets the rule of LL index.

As shown in Fig. S7(a), the strain-free armchair MoS_2NR [6] has a direct band gap about 2.18 eV. Under bending, the CBs shift down and VBs shift up, leading to a reduced band gap about 1.56 eV. Moreover, the wave functions of bent MoS_2NR are well localized at the edge of the NR, see Fig. S7(b). Similar to zigzag NRs, the number of nodes of the localized electronic states also meets the rule of LL index.

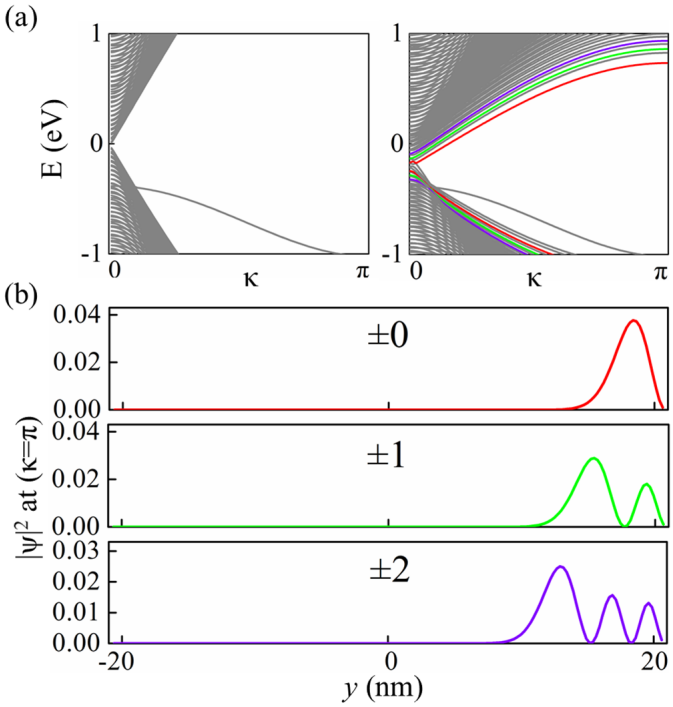

FIG. S2. (a) Electronic band structure of a 40 nm-wide armchair GNR with bending angle $\Omega = 0^\circ$ (left)[strain-free] and $\Omega = 0.18^\circ$ (right). (b) Spatial distributions of wave functions along width direction x for the first three LLs ($n = \pm 0, \pm 1, \pm 2$) at $\kappa = \pi$. The wave functions in red, green, and purple colors corresponding to the bands highlighted with the same colors as shown in (a).

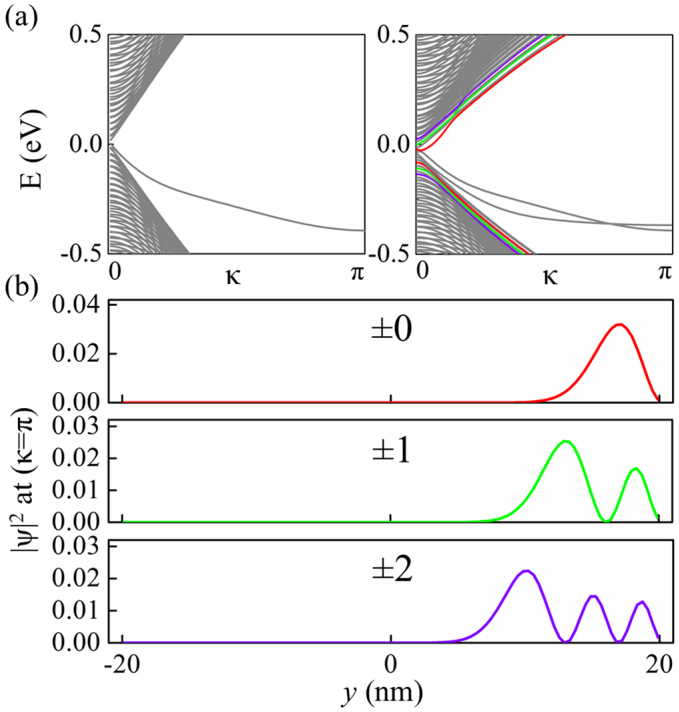

FIG. S3. (a) Electronic band structure of a 40 nm-wide armchair SiNR with bending angle $\Omega = 0°$ (left)[strain-free] and $\Omega = 0.18°$ (right). (b) Spatial distributions of wave functions along width direction x for the first three LLs ($n = \pm0, \pm1, \pm2$) at $\kappa = \pi$. The wave functions in red, green, and purple colors corresponding to the bands highlighted with the same colors as shown in (a).

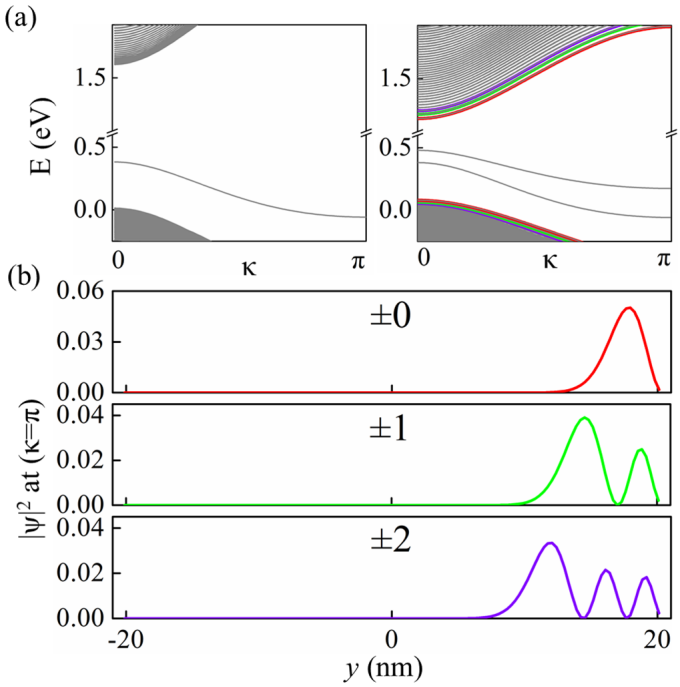

FIG. S4. (a) Electronic band structure of a 40 nm-wide armchair SiCNR with bending angle $\Omega = 0°$ (left)[strain-free] and $\Omega = 0.15°$ (right). (b) Spatial distributions of wave functions along width direction x for the first three LLs ($n = \pm0, \pm1, \pm2$) at $\kappa = \pi$. The wave functions in red, green, and purple colors corresponding to the bands highlighted with the same colors as shown in (a).

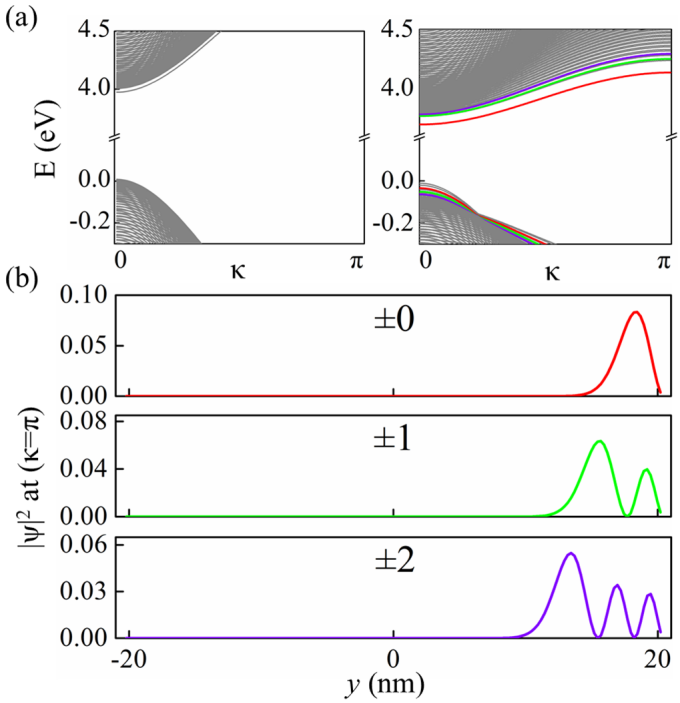

FIG. S5. (a) Electronic band structure of a 40 nm-wide armchair BNNR with bending angle $\Omega = 0°$ (left)[strain-free] and $\Omega = 0.12°$ (right). (b) Spatial distributions of wave functions along width direction x for the first three LLs ($n = \pm0, \pm1, \pm2$) at $\kappa = \pi$. The wave functions in red, green, and purple colors corresponding to the bands highlighted with the same colors as shown in (a).

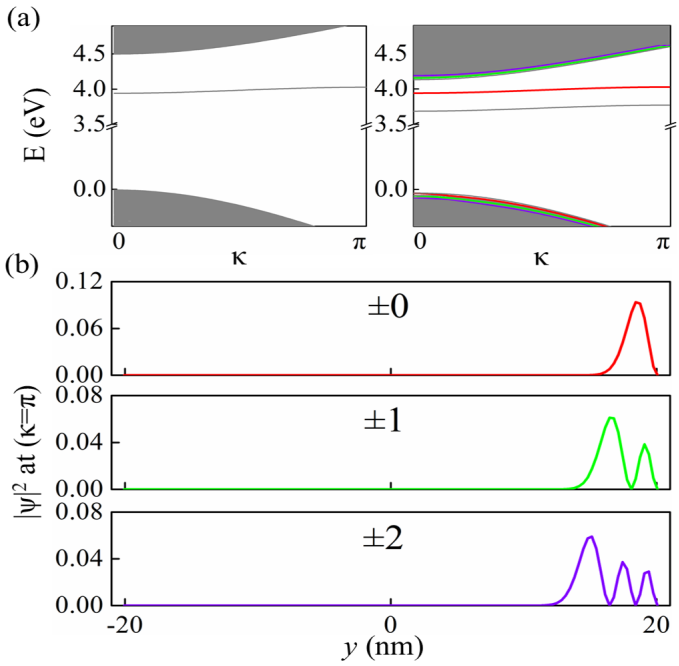

FIG. S6. (a) Electronic band structure of a 40 nm-wide armchair ZnONR with bending angle $\Omega = 0°$ (left)[strain-free] and $\Omega = 0.06°$ (right). (b) Spatial distributions of wave functions along width direction x for the first three LLs ($n = \pm0, \pm1, \pm2$) at $\kappa = \pi$. The wave functions in red, green, and purple colors corresponding to the bands highlighted with the same colors as shown in (a).

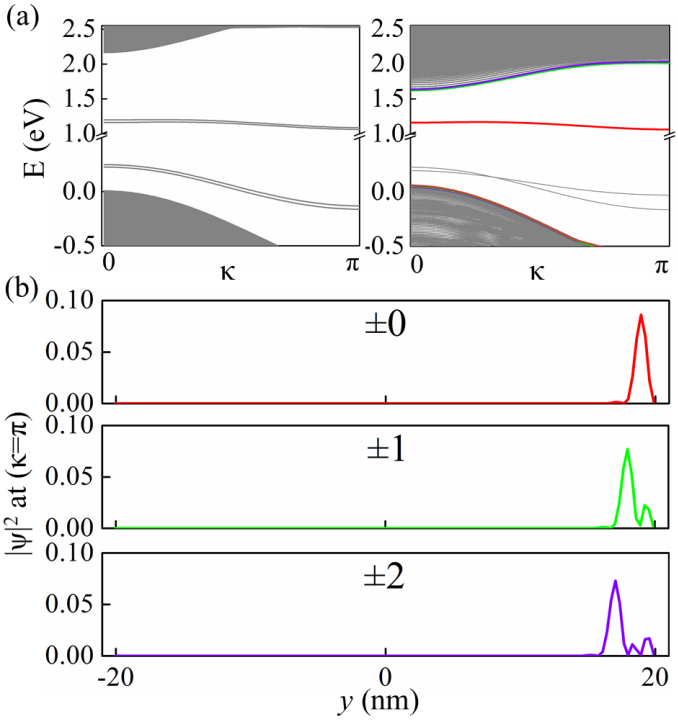

FIG. S7. (a) Electronic band structure of a 40 nm-wide armchair MoS_2NR with bending angle $\Omega = 0^\circ$ (left)[strain-free] and $\Omega = 0.06^\circ$ (right). (b) Spatial distributions of wave functions along width direction x for the first three LLs ($n = \pm 0, \pm 1, \pm 2$) at $\kappa = \pi$. The wave functions in red, green, and purple colors corresponding to the bands highlighted with the same colors as shown in (a).

III. RELATIVE ENERGY $E_0 - E_0^0$ OF THE ARMCHAIR NANORIBBONS VERSUS THE BENDING ANGLE

Here, we show the relationship between the relative energy $E_0 - E_0^0$ at $\kappa = \pi$ and the bending angle Ω for the armchair NRs. As shown in Fig. S8, the results indicate the same linear relationship.

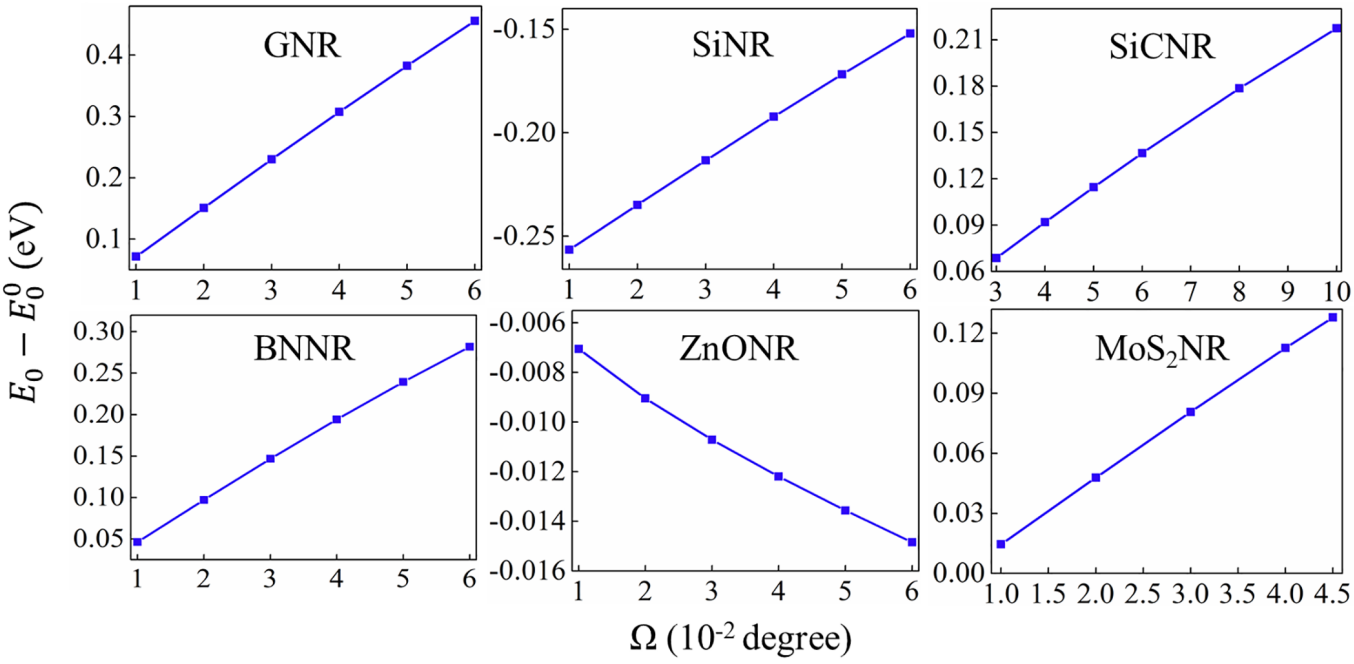

FIG. S8. Relative energy $E_0 - E_0^0$ at $\kappa = \pi$ versus bending angle Ω for bent armchair NRs.

* Corresponding author; zliu@hebtu.edu.cn
† Corresponding author; jtsong@hebtu.edu.cn

[1] G. Gui, D. Morgan, J. Booske, J. Zhong and Z. Ma, Applied Physics Letters, 2015, **106**, 053113.
[2] E. Zaminpayma and P. Nayebi, Physica E: Low-dimensional Systems and Nanostructures, 2016, **84**, 555–563.
[3] B.-L. Gao, Q.-Q. Xu, S.-H. Ke, N. Xu, G. Hu, Y. Wang, F. Liang, Y. Tang and S.-J. Xiong, Physics Letters A, 2014, **378**, 565–569.
[4] Q. Peng, Nanotechnology, 2018, **29**, 405201.
[5] M. Topsakal, S. Cahangirov, E. Bekaroglu and S. Ciraci, Phys. Rev. B, 2009, **80**, 235119.
[6] E. Scalise, M. Houssa, G. Pourtois, V. Afanas'ev and A. Stesmans, Nano Research, 2012, **5**, 43–48.